PROC. OF JSCE,
No. 204, AUG. 1972

LOAD CARRYING CAPACITY OF TWO HINGED STEEL ARCHES

By Shigeru KURANISHI and Le-Wu LU***

1. INTRODUCTION

In the recent years, many studies have been made on the load-carrying capacity of arches that fail in the plane of the applied load. In chronological order, these studies may be divided into three phases. The problem studied in the first phase is concerned with the elastic buckling of arches stressed in pure compression or in combined compression and bending. The solutions obtained permit an evaluation of the strength of very slender arches. The second phase deals with the plastic failure of arches after the formation of a sufficient number of plastic hinges. In the third phase the combined influence of buckling and yielding is considered, and the solutions thus developed provide the best estimate of the load-carrying capacity of arches.

The problem of elastic buckling of arches has been studied by a number of investigators, among them Dinnik[2], Stüssi[2], and Ratzersdorfer[3]. Stüssi, applying the Vianello-Engesser method, computed the buckling load for fixed, two-hinged, and three-hinged parabolic arches of different rise-to-span ratios. Tests on model steel arches were carried out by Gaber[4] and Kollbrunner[5] and close correlation between the experimental and theoretical buckling loads was found. In 1940 Deutsch reported the results of a series of tests on prismatic and non-prismatic arches subjected to unsymmetrical vertical loads[6]. The results indicate that unsymmetrical loading tends to cause instability failure at much lower values of the horizontal thrust than does symmetrical loading. The reduction in horizontal thrust can be attributed, at least, in part, to the vertical and horizontal deflection effects existing in the arches in the case of unsymmetrical loading. But the ultimate load intensity is nearly equal for the the both cases. A comprehensive survey of the literature on arch buckling has been prepated by Austin[7].

The behavior and strength of arches in the plastic range have been studied theoretically and experimentally by Swida[8], Hendry[9], Johansen[10], Lange Hansen[11], and Steven[12]. In 1953, Onat and Prager[13] presented a general method of solution that took into account the plastic hinge action under combined bending and axial thrust. In some of the tests carried out by Johansen, it was found that when the applied load caused axial compression along the arch the experimentally observed ultimate loads were lower than the theoretical predictions. Johansen also reported that the load-carring capacity of the test arches was significantly increased when the direction of the applied load was reversed. In this case axial tension existed in the arch and failure due to instability could not occur. The latter problem was studied in detail by Onat and Shu[14] who used the splitting plastic hinge concept and included the effect of deformations in formulating their solutions. A study was made by Yamazaki and Ishikawa[15] of the influence of the spread of plastic zones on the deflection of circular arches.

Very limited works have been carried out to study the strength of arches by considering the combined influence of instability and yielding. In 1970, Harries[16] presented the results of an analytical study on slender arches with rectangular and circular (tube) cross sections using a similar iterative method to that of this paper. He discussed the buckling problem and used his results to examine the adequacy of the provisions contained in the German Specification (DIN 4114). In the same year Maeda and Fujimoto[17] reported the results of their study which also consider-

* Dr. Eng. Associate Professor, Department of Civil Engineering, Faculty of Engineering, Tohoku University.

** Ph.D. Professor of Civil Engineering, Fritz Engineering Laboratory, Lehigh University.

ed the formation of concentrated plastic hinges.

In this paper a numerical method is developed to study the load carrying capacity of arches, including the effects of spread of yielding and finite deformations. The method is applied to the analysis of parabolic arches with rectangular and sandwich cross sections. Also included in the formulation of the method are the rough estimation of the effects of residual stresses and strain hardening of the material for sandwich cross sections. An outline of this paper was presented at the annual meeting of JSCE in 1970. A comparison of the results obtained by Harris[16] with those of this paper is shown later in Fig. 24.

2. FORMULATION OF THE METHOD

(1) Assumptions

The following assumptions that are often made in routine structural analysis are adopted in the development of the proposed method.

1. All plane sections along the arch remain plane after loading (Bernoulli-Euler's hypothesis).
2. The deformations are comparatively small and the effect of shortening of the arch axis to the curvature of the arch is negligible.
3. Non-linear stress distribution in a cross section due to the curvature of arch axis is negligible.
4. The stress increases monotonically to the ultimate state. The effect of the elastic unloading caused by stress reversals is not considered.
5. The effect of shear stresses on the deformation and the formation of plastic zones is neglected.
6. The arch is made of material whose stress-strain characteristic is elastic and perfectly plastic. A linear strain-hardening relationship is used in the analysis of arches with sandwich cross sections.

(2) The Iterative Approach

The arches considered in this paper are statically indeterminate structures whose analysis usually requires consideration of deformation. The distribution of bending moment and axial thrust along the arch is determined from the compatibility requirements of the deformation. This is usually a straightforward procedure if the arch remains elastic and the effect of finite deformation is ignored. The occurrence of yielding at a section causes a change in the moment vs. curvature relationship, which, in turn, affects the deformations of the arch. The inclusion of the effect of finite deformation requires that the bending moment is to be computed for the deformed configuration of the arch. Thus, the bending moment distribution and the deformation become mutually dependent and a direct solution of the problem is almost impossible.

The deformation of the arch axis is defined by its moment vs. curvature and thrust vs. axial shortening (or elongation) relationships. Fig. 1 shows a set of the interaction relationships computed for a rectangular section. The dotted lines

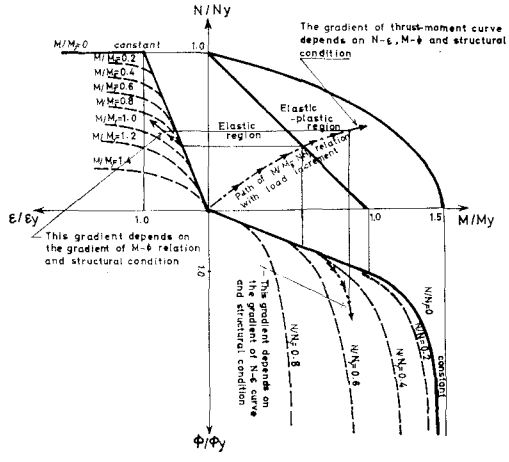

Fig. 1 Interaction curve of M-N-ϕ-ε relationship.

in the second quadrant represent the N-ε relationships for constant values of the applied moment, and those in the fourth quadrant are the M-ϕ curves corresponding to constant values of the axial thrust. Therefore, the curvature ϕ depends not only on the applied moment but also on the

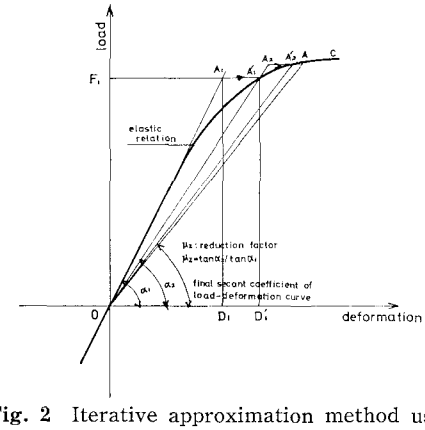

Fig. 2 Iterative approximation method used in this paper.

axial thrust. Both the moment and the axial thrust must be determined from deformation considerations.

Because of the complexity of the interaction relationships and the difficult of directly including the effect of deformation in the analysis, an iterative approach was developed for this investigation. This approach is illustrated in Fig. 2. The actual load vs. deformation relationship of the arch is shown by curve OC with the initial portion representing the elastic response. The first set of computations assumes the arch to remain elastic and neglects the effect of deformation. For the load F_1, a point A_1 is obtained with the corresponding deformation defined by point D_1. However, the true deformation corresponding to this load is given by A_1' on curve OC. A second set of computation is then made, using a stiffness reduction factor $\mu=\tan\alpha_2/\tan\alpha_1$ and including the deformation determined from the first set of computation. A point A_2 is then obtained. The process is repeated until the computation finally converges to the desired point on the load-deformation curve.

(3) Computation for the Effect of Deformation

The procedure to account for the effect of deformation can be explained with reference to the two-hinged parabolic arch as shown in Fig. 3. The first step in the iterative procedure is to

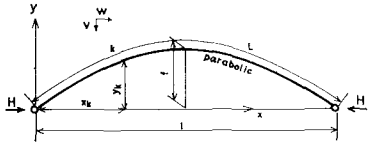

Fig. 3

compute the bending moment, the horizontal reaction and the resulting deformation, using the conventional elastic theory. The effect of deformation is ignored in the initial computation. In the next step the secondary bending moment and horizontal reaction caused by the deformation of the arch axis are computed using the deformation obtained in the first step. The procedure is repeated until the secondary quantities obtained from the computations become negligibly small. This procedure is illustrated in Fig. 4. When the arch is loaded by a distributed load of intensity q, the vertical reaction R_A at the left support is given by

$$R_A=\int_0^1 q(1-x)dx \qquad \cdots\cdots(1)$$

The initial bending moment, horizontal reaction

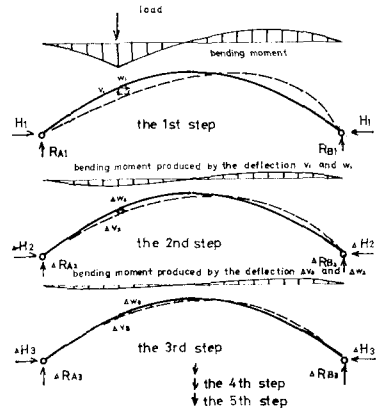

Fig. 4 Calculation of the influence of the finite deformations by the iterative method.

and deflection of the arch can be determined from the following equations

$$M=M_0-Hy \qquad \cdots\cdots(2)$$

$$H=\frac{\int_0^1 \frac{M_0 y}{\mu\alpha\sin\gamma}dx}{\int_0^1\left(\frac{y^2}{\mu\alpha\sin\gamma}+\frac{1}{\nu\lambda^2\sin^3\gamma}\right)dx} \qquad \cdots\cdots(3)$$

$$\left.\begin{aligned} v_k&=\left(\frac{l^2}{EI_c}\right)\int_0^1\left\{\frac{M(M_{0k}-H_k y)}{\mu\alpha\sin\gamma}+\frac{H\,H_k}{\nu\lambda^2\sin^3\gamma}\right\}dx\\ w_k&=\left(\frac{l^2}{EI_c}\right)\int_0^1\left\{\frac{M(M_{0wk}-H_{wk}y)}{\mu\alpha\sin\gamma}+\frac{H(H_{wk}+\mathrm{Step}_x^{x_k})}{\nu\lambda^2\sin^3\gamma}\right\}dx\end{aligned}\right\} \qquad \cdots\cdots(4)$$

in which

$$\left.\begin{aligned} H_k&=\frac{\int_0^1\frac{M_{0k}y}{\mu\alpha\sin\gamma}dx}{\int_0^1\left(\frac{y^2}{\mu\alpha\sin\gamma}+\frac{1}{\nu\lambda^2\sin^3\gamma}\right)dx}\\ H_{wk}&=\frac{\int_0^1\left(\frac{M_{0wk}y}{\mu\alpha\sin\gamma}-\frac{\mathrm{Step}_x^{x_k}}{\nu\lambda^2\sin^3\gamma}\right)dx}{\int_0^1\left(\frac{y^2}{\mu\alpha\sin\gamma}+\frac{1}{\nu\lambda^2\sin^3\gamma}\right)dx}\end{aligned}\right\} \qquad \cdots\cdots(5)$$

$$\left.\begin{aligned} M_{0k}&=(1-x_k)x-\mathrm{Step}_x^{x_k}(x-x_k)\\ M_{0wk}&=-(y_k x)+\mathrm{Step}_x^{x_k}(y-y_k)\end{aligned}\right\} \qquad \cdots\cdots(6)$$

In the above equations, μ and ν are the reduction factors for bending stiffness and axial stiffness (shortening or elongation), I_c a moment of

inertia used for reference purpose, λ the slenderness ratio of the arch with I_c, $\alpha=I/I_c$, γ the angle of inclination, and $\mathrm{Step}_x^{x_k}$ denotes a step function.

The increment of the vertical reaction ΔR_A due to the horizontal deflection w is

$$\Delta R_A=-\int_0^1 qw\,dx\,. \qquad \cdots\cdots(7)$$

The increment of the bending moment ΔM_0 caused by the vertical and horizontal deflections v and w is

$$\Delta M_0=Hv+(\Delta R_A\bar{x}+R_Aw)-\int_0^x q(w_{(x_k)}-w_{(x)})dx_k \qquad \cdots\cdots(8)$$

and the increment of the horizontal reaction is

$$\Delta H=\frac{\displaystyle\int_0^1\frac{\bar{y}}{\mu\alpha\sin\bar{\gamma}}\Delta M_0\,dx}{\displaystyle\int_0^1\left(\frac{\bar{y}^2}{\mu\alpha\sin\bar{\gamma}}+\frac{1}{\nu\lambda^2\sin\bar{\gamma}}\right)dx} \qquad \cdots\cdots(9)$$

in which $\bar{x}$, $\bar{y}$ are the coordinates and $\bar{\gamma}$ the angle of inclination of the arch axis in the deformed position. The secondary bending moment ΔM is given by

$$\Delta M=\Delta M_0-\Delta H\bar{y} \qquad \cdots\cdots(10)$$

The secondary moment and horizontal reaction can be used to compute the deflections Δv_k and Δw_k caused by v and w

$$\left.\begin{aligned}\Delta v_k&=\left(\frac{l^2}{EI_c}\right)\int_0^1\left\{\frac{1}{\mu\alpha\sin\bar{\gamma}}(\Delta M\cdot\bar{M}_k)+\frac{\Delta H\cdot\bar{H}_k}{\nu\lambda^2\sin\bar{\gamma}}\right\}dx\\ \Delta w_k&=\left(\frac{l^2}{EI_c}\right)\int_0^1\frac{1}{\mu\alpha\sin\bar{\gamma}}(\Delta M\cdot\bar{M}_{wk})+\frac{\Delta H(\bar{H}_{wk}+\mathrm{Step}_x^{x_k})}{\nu\lambda^2\sin\bar{\gamma}}\end{aligned}\right\} \qquad \cdots\cdots(11)$$

The quantities $\bar{H}_k$, $\bar{H}_{wk}$, $\bar{M}_k$, and $\bar{M}_{wk}$ which are to be used in the above equations can be obtained from Eqs. (5) and (6) by replacing x, y and γ by $\bar{x}$, $\bar{y}$ and $\bar{\gamma}$. When Δv and Δw are substituted into Eqs. (7), (8), (9) and (10), a new set of the secondary quantities are obtained. The computations may be terminated when the increments of the secondary quantities become sufficiently small.

(4) Computation for the Effect of Plastification

The effect of yielding on the deflections and the internal force distribution of the arch can be included in the computations by using the stiffness reduction factors μ and ν. The reduction factors are evaluated by the secant modulus concept as shown in Fig. 2. Both μ and ν are defined as the ratio of the secant coefficient to the elastic coefficient. At low levels of the applied load, the arch is completely elastic and μ and ν are both equal to unity. As the applied load increases, partial yielding will occur in certain sections of the arch, causing a reduction of the values of μ and ν. In general, μ and ν can be determined only after the values of the bending moment and axial thrust are known.

Since the numerical results to be presented later in this paper are for arches with rectangular and sandwich sections, it is necessary to discuss briefly the reduction factors μ and ν for these sections. Jezek[18] has shown that the stress state in a rectangular section can be classified into three different cases if the material is assumed to be elastic and perfectly plastic (no strain hardening). The three cases are given in Table 1 together with the moment-thrust-curvature relationship applicable to each case. All the quantities are expressed nondimensionally with the ratio ζ defining the distance between the neutral axis and the centroidal axis of the cross section. The reduction factors are given by

Table 1 M-N-ϕ-ζ relations for rectanglar cross section

Case	Stress state	Condition	Calculation formula for ϕ & ζ
I	Elastic	$0<\bar{M}_y\leqslant 1-\bar{N}_y$	$\bar{\phi}_y=\bar{M}_y$
			$\zeta=1/2\cdot\bar{N}_y\bar{\phi}_y$
II	Fiber stress is yielded on one side	$1-\bar{N}_y<\bar{M}_y\leqslant(1+2\bar{N}_y)(1-\bar{N}_y)$	$\bar{\phi}_y=4(1-\bar{N}_y)^3\{3(1-\bar{N}_y)-\bar{M}_y\}^{-2}$
			$\zeta=1/2\cdot(1+1/\bar{\phi}_y)+\sqrt{1-\bar{N}_y/\bar{\phi}_y}$
III	Fiber stress is yielded on both side	$(1+2\bar{N}_y)(1-\bar{N}_y)<\bar{M}_y\leqslant 3/2\cdot(1-\bar{N}_y^2)$	$\phi_y=1/\sqrt{3(1-\bar{N}_y^2)-2\bar{M}_y}$
			$\zeta=\bar{N}_y/2$
Rectangular cross section, $\bar{\phi}_y=\phi/\phi_y$, $\bar{M}_y=M/M_y$, $\bar{N}_y=N/N_y$			

$$\mu=\frac{\phi_y}{\phi}\frac{M}{M_y}, \qquad \nu=\frac{1}{2\zeta}\frac{N}{N_y}\frac{\phi_y}{\phi} \qquad \cdots\cdots(12)$$

in which

$$\phi_y=\frac{2\varepsilon_y}{h}, \quad M_y=\frac{bh^2\sigma_y}{6} \quad \text{and} \quad N_y=bh\sigma_y .$$

For the sandwich section, it is possible to include both the effects of residual stress and strain hardening. The residual stress distribution assumed in this study is shown in Fig. 5.

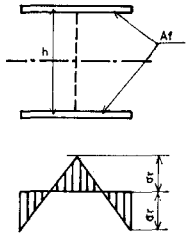

Fig. 5 Distribution of residual stress in flanges.

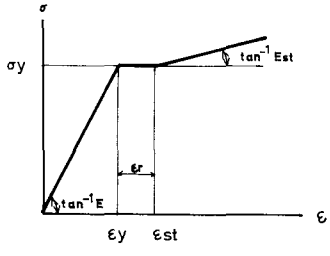

Fig. 6 Stress-strain curve.

The magnitude of the residual stresses in the cross section is defined by the flange tip stress σ_r. The stress-strain relationship is assumed to be elastic, perfectly plastic and linear strain hardening (Fig. 6). The strain-hardening modulus E_{st} defines the slope of the stress-strain curve at the onset of strain hardening. For the assumed residual stress distribution and the linear strain hardening property, it can be shown that the total number of possible stress states is

Table 2

Case	Stress state	Condition
I-1	Both flanges are elastic	$0\leqslant S_p\leqslant e$, $0<D_p\leqslant e$
I-2		$0\leqslant S_p\leqslant e$, $0>D_p\leqslant -e$
II-1	One flange is partially yielded the other flange is elastic	$e<S_p\leqslant 1$, $0\leqslant D_p\leqslant e$
II-2		$e<S_p\leqslant 1$, $0>D_p\leqslant -e$
III-1	Both flanges are partially yielded	$e<S_p\leqslant 1$, $e<D_p\leqslant 1$
III-2		$e<S_p\leqslant 1$, $-e\geqslant D_p\geqslant -1$
IV-1	One flange is fully plastic the other flange is elastic	$1<S_p$, $0\leqslant D_p\leqslant e$
IV-2		$1<S_p$, $0>D_p\geqslant -e$
V-1	One flange is fully plastic the other is partially yielded	$1<S_p$, $e\leqslant D_p\leqslant 1$
V-2		$1<S_p$, $-e\geqslant D_p\geqslant -1$
VI-1	Both flanges are fully plastic	$1\leqslant S_p$, $1\leqslant D_p$
VI-2		$1\leqslant S_p$, $-1\geqslant D_p$

$S_p=|M|/M_p+|N|/N_p$, $D_p=|M|/M_p-|N|/N_p$

Table 3 M-N-ϕ-ζ relation for a sandwich cross section

Case	$\bar{\phi}_y$	ζ
I-1	M/M_p	$N/\bar{\phi}_y N_y$
I-2	〃	
II-1	$1-e/2+D_p/2-\sqrt{1-e}\sqrt{1-S_p}$	$1/2-D_p/2\bar{\phi}_y$
II-2	〃	
III-1	$(2-e)-\sqrt{1-e}\sqrt{1-S_p}+\sqrt{1-D_p}/2$	$\{(1-e/2)-\sqrt{1-e}\sqrt{1-S_p}\}/\bar{\phi}_y-1/2$
III-2	$\{\sqrt{1+D_p}-\sqrt{1-S_p}\}\sqrt{1-e}$	
IV-1	$(1-e/2)+(S_p-1)/2\tau_{st}+D_p$	$\{(1-e/2)+(S_p-1)/2\tau_{st}\}/\bar{\phi}_y-1/2$
IV-2	〃	
V-1	$(S_p-1)/2\tau_{st}+(2-e)-\sqrt{1-e}\sqrt{1-D_p}$	$\{(1-e/2)+(S_p-1)/2\tau_{st}\}/\bar{\phi}_y-1/2$
V-2	$(S_p-1)/2\tau_{st}+\sqrt{1-e}\sqrt{1+D_p}$	
VI-1	$M/M_p\tau_{st}+(2-e)-1/\tau_{st}$	$\{(1-e/2)+(S_p-1)/2\tau_{st}\}/\bar{\phi}_y-1/2$
VI-2	$M/M_p\tau_{st}$	

$\bar{\phi}_y=e\phi/\phi_y$ ($\phi_y=2e\varepsilon_y/h$), $M_p=A_f\sigma_y h$, $N_y=2A_f\sigma_y$, $e=1-\sigma_r/\sigma_y$ and $\tau_{st}=E_{st}/E$

12. These stress states and the corresponding conditions are listed in Table 2 and the M-N-ϕ-ζ relationships are given in Table 3. The reduction factors for the sandwich section are

$$\mu=\frac{\phi_y}{\phi}\frac{M}{M_p}, \qquad \nu=\frac{1}{2\zeta}\frac{N}{N_y}\frac{\phi_y}{\phi} \qquad \cdots\cdots(13)$$

in which

$$M_p=A_f h\sigma_y, \quad N_p=2A_f\sigma_y, \quad \phi_y=\frac{2\sigma_y}{Eh}e$$

and $$e=1-\frac{\sigma_r}{\sigma_y}.$$

(5) Procedure for Numerical Computation

For convenience of computation, the uniformly distributed load q is replaced by a series of closely spaced concentrated loads. The basic equations of equilibrium and displacements can be integrated numerically using the iterative method described above. Initially, all sections of the arch are assumed to be elastic ($\mu=\nu=1.0$). After several cycles of iteration, satisfactory convergence can usually be established for the values of bending moment M and axial thrust N existing at all sections along the arch. If the combination of M and N at a section exceeds that specified for Case I of Tables 1 or 2, partial yielding will occur at this section. The reduction factors μ and ν applicable to the section can be estimated from the bending moments and axial thrust obtained at the end of the iterative calculations. The μ and ν values determined for all the sections (elastic or partially plastic) are substituted into the basic equations, and their solutions may again be obtained by iterations. The process is repeated until the μ and ν values obtained in two successive sets of computations converge. When this occurs, a point on the load-deformation curve of the arch can be established. The applied load is then increased and the whole procedure is repeated. The load will reach its ultimate value when: (a) the deformations found in the iterative computations begin to diverge or (b) the bending moment and axial thrust combinations fall beyond those corresponding to the nearly fully plastic stress state. For the arches analyzed in this paper, it has been found that both situations could develop. A summary of the ultimate conditions of the arches studied is given in Table 4, in which "Def. Div." and "B.M." denote, respectively, "deflection divergence" and "beyond maximum".

Table 4

λ \ ε	0	0.25	0.5	0.75	0.99
75	B.M.	B.M.	B.M.	B.M.	B.M.
100	B.M.	B.M.	B.M.	B.M.	Def. Div.
150	B.M.	B.M.	Def. Div.	Def. Div.	Def. Div.

For convenience of computation, the arch is divided into 40 segments. The accuracies aimed at in the analysis are 1% for the deflections v and w, 5% for the reduction factors μ and ν, and 0.5% for the ultimate load.

3. PRESENTATION OF RESULTS

Numerical computations have been carried out for parabolic arches of different rise-to-span ratios (f/l) and with rectangular and sandwich cross sections. An important parameter considered in the study is the slenderness ratio which is defined as ratio of the radius of gyration of the cross section to the overall length of the arch. All computations are performed for the loading conditions shown in Fig. 7. The load parameter in this figure defines the magnitude of the applied load for the right-hand half of the arch.

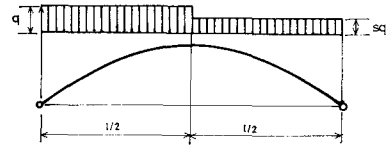

Fig. 7 Unsymmetrical loading.

By varying the value of s, it is possible to study the influence of unsymmetrical loading on the strength of the arches. As mentioned in the "Introduction", the load-carrying capacity for the unsymmetrical case is usually lower than that for the symmetrical case. In presenting the results, the applied load is expressed non-dimensionally by the ratio q/q_p, in which q_p is the magnitude of the uniformly distributed load (covering the entire arch) that will cause the arch to yield by axial thrust, at the springings by the 1st order analysis. For parabolic arches, q_p is given by

$$q_p=\frac{2A\sigma_y}{l\sqrt{\frac{1}{16}\left(\frac{l}{f}\right)^2+1}} \qquad \cdots\cdots(14)$$

The material properties and the magnitude of residual stresses assumed in the computations are as follows: $\sigma_y=2\,400\ \mathrm{kg/cm^2}$, $E=2.1\times10^6\ \mathrm{kg/cm^2}$, $E/E_{st}=50$, and $\sigma_r=0.3\ \sigma_y$.

Fig. 8 shows the relationships between the applied load and the resulting deflection at the

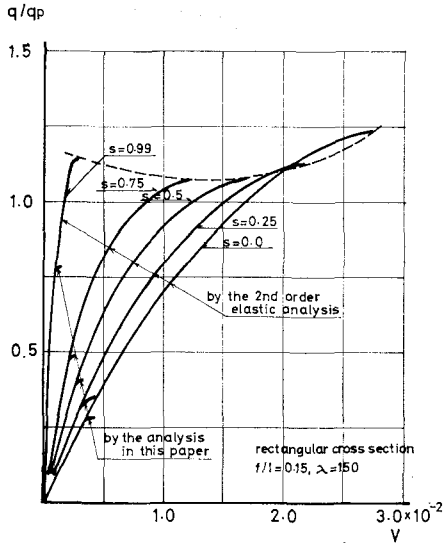

Fig. 8 Load-deflection curves.

quarter point of an arch with $f/l=0.15$ and $\lambda=150$. The cross section of the arch is rectangular. Two sets of load-deflection curves are presented both in including the effect of deflections. One set assumes that the no yielding occurs in the arch and the other considers the influence of yielding. The load-deflection curves determined for the elastic condition show that the maximum load does not vary appreciably with s. However, if yielding is allowed to develop, the carrying capacity of the arch will be substantially lowered as the applied load becomes unsymmetrical. The former observation is consistent with that reported by Deutsch[6] based on his experimental results. The reduction in strength for the unsymmetrical loading condition is due mainly to the increased influence of bending moment which tends to cause more yielding in the arch. This point is illustrated by the results of

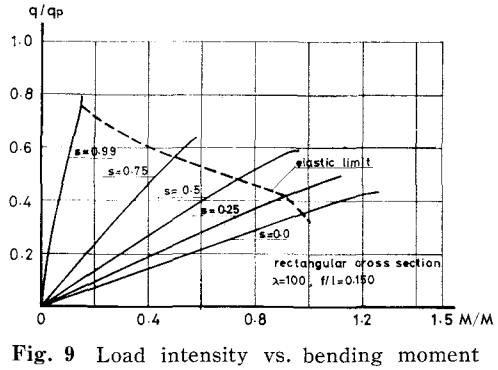

Fig. 9 Load intensity vs. bending moment relationships at quarter point.

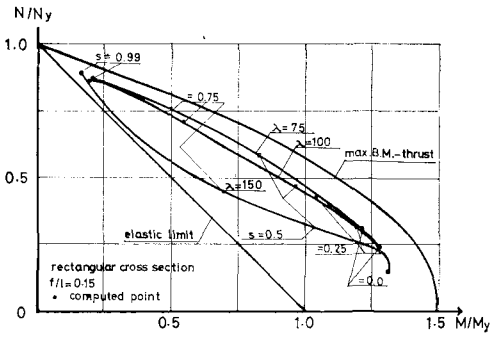

Fig. 10 N/N_y-M/M_y combinations at quarter point of arches for various s values (applied load=$q_{\max}$).

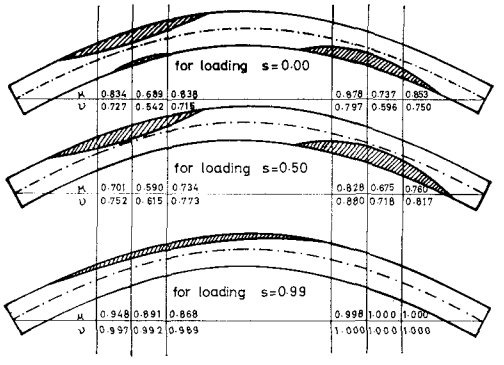

Fig. 11 Yielded zones and reduction factors.

Figs. 9, 10, and 11 which were obtained for an arch with different rigidity as that of Fig. 8 (same f/l but with $\lambda=100$). Fig. 9 shows the relationships between the applied load and the bending moment at the left quarter point. As may be expected, the bending moment increases appreciably as s decrease from 0.99 to 0. The combinations of bending moment and axial thrust at the most stressed point of the arch for various unsymmetrical loading conditions are given in Fig. 10. All results are for the ultimate state with $q=q_{\max}$. Also shown in the figure are similar results obtained for the arch referred to in Fig. 8 ($\lambda=150$) and for an additional arch with $\lambda=75$. For each curve the highest point represents the combination of M and N occurring at the quarter point for $s=0.99$, and the lowest point gives the M and N values for $s=0$. Fig. 11 shows the yielded zones and the stiffness reduction factors of the arch ($\lambda=100$) at the ultimate state for three loading conditions with $s=0$, 0.5 and 0.99.

The deflection of the three arches at the maximum load $v_{\max}$ are plotted against the load para-

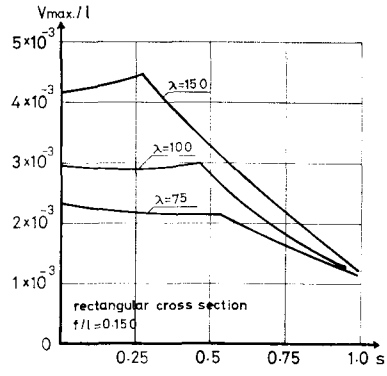

Fig. 12 Max. deflection at the ultimate state.

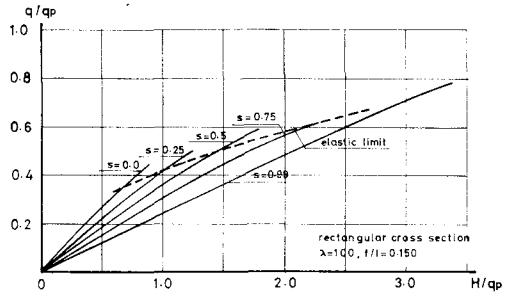

Fig. 13 Load intensity vs. horizontal thrust relationships.

meter s in Fig. 12. In general, maximum load deflection increases as the loading pattern becomes more and more unsymmetrical. This is due to the fact that deflection is produced primarily by bending moment. The loading condition that produces more bending moment in the arches usually would cause larger deflections.

Fig. 13 shows the relationships between the applied load and the horizontal thrust (support reaction) of the arch with $f/l=0.15$ and $\lambda=100$. Because of the inclusion of the deformation effect, the results obtained are always non-linear even at low levels of the applied load.

Extensive computations have been carried out for arches with different slenderness ratios and rise-to-span ratios. For each arch, a full range of s values was assumed. The purpose of these computations is to study the influence of the three parameters (s, λ, and f/l) on the load-carrying capacity of the arches. The maximum loads obtained for arches with rectangular cross section are summarized in Figs. 14, 15, 16 and 17, and those for sandwich arches in Figs. 18, 19, 20 and 21. On a non-dimensional basis, the results for the sandwich arches are not significantly different from those for the rectangular cross section arches. Figs. 14 and 18 give an additional support to the previous observation that the load-carrying capacity of a arch de-

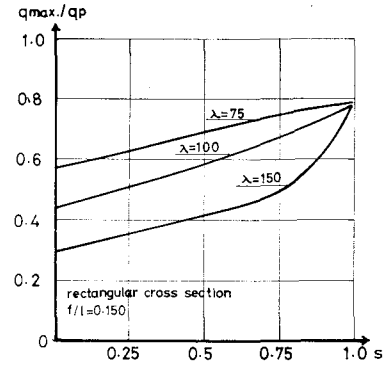

Fig. 14 Relationships between maximum load intensity and load parameter (constant f/l ratio).

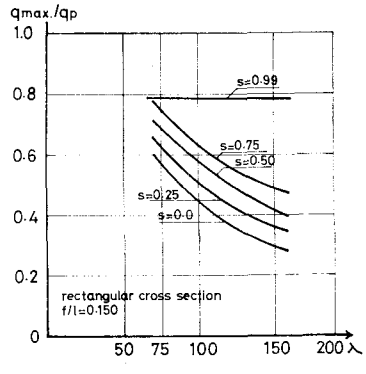

Fig. 15 Relationships between maximum load intensity and slenderness ratio (constant f/l ratio).

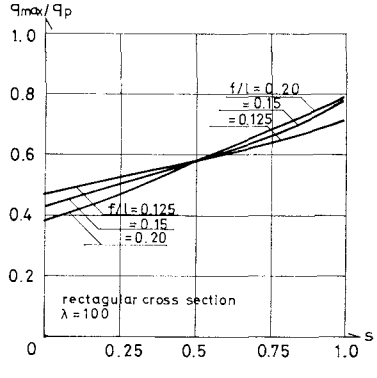

Fig. 16 Relationships between maximum load intensity and rise span ratio (constant λ).

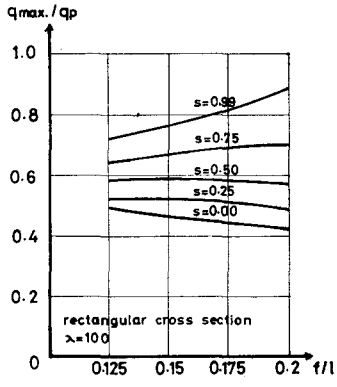

Fig. 17 Relationships between maximum load intensity and rise-to-span ratio.

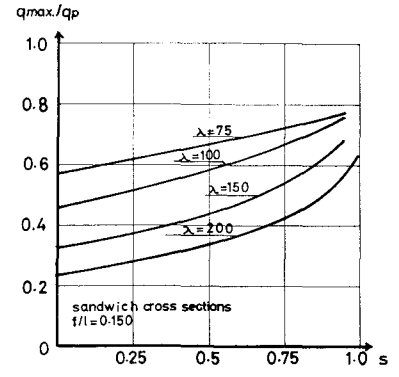

Fig. 18 Relationships between maximum load intensity and load parameter (constant f/l ratio).

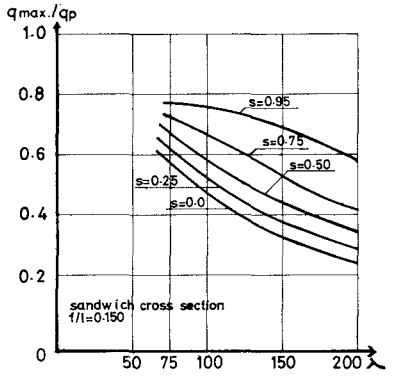

Fig. 19 Relationships between maximum load intensity and slenderness ratio (constant f/l ratio).

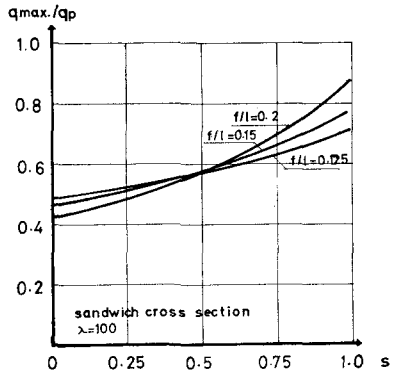

Fig. 20 Relationships between maximum load intensity and load parameter (constant λ).

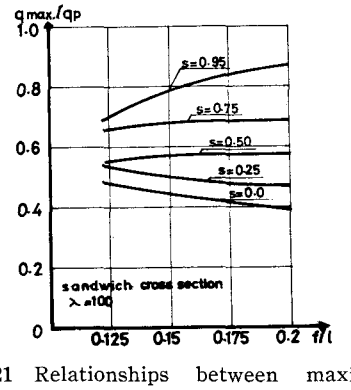

Fig. 21 Relationships between maximum load intensity and rise-to-span ratio.

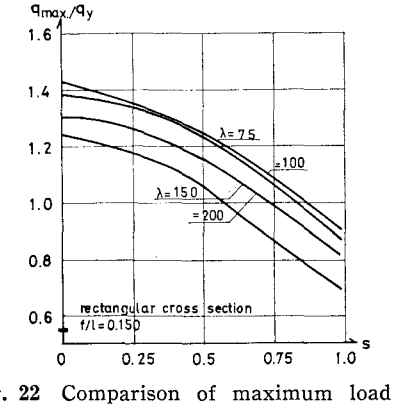

Fig. 22 Comparison of maximum load intensity with elastic limit load (constant f/l ratio).

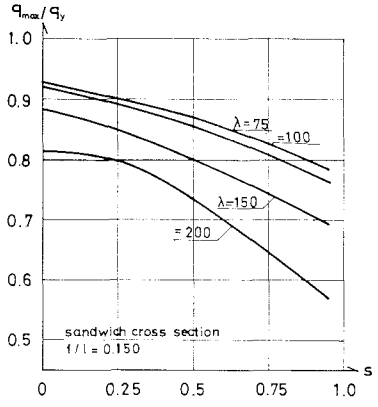

Fig. 23 Comparison of maximum load intensity with elastic limit load (constant f/l ratio).

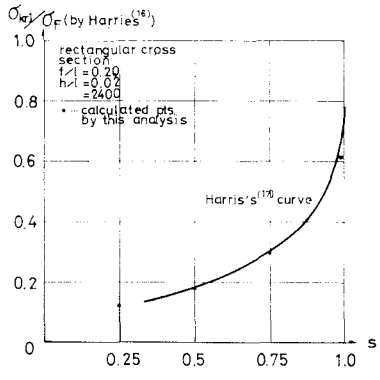

Fig. 24 A comparison with the result given by Harris[17].

creases as the applied load becomes unsymmetrical ($s \to 0$). For the rectangular section arches, the load carrying capacity reaches a maximum value of 0.8 q_p as s approaches 1.0 (symmetrical loading). The results presented in Figs. 14 to 21 also show that

1. For a given loading pattern (constant s), the maximum load decreases as the slenderness ratio increases, indicating the importance of instability effect in slener arches.
2. For arches of constant slenderness ratio, the ratio of q_{max}/q_p increases with the rise-to-span ratio for large s values, but the trend reverses for small s values.

The results of Figs. 14 and 18 are replotted in Figs. 22 and 23 with the maximum load q_{max} non-dimensionalized with respect to the initial yield (or elastic limit) load q_y. This load is computed by using the conventional elastic theory which neglects the effect of finite deflections; it is usually used the basis for elastic design. Contrary to the trend observed previously, Figs. 22 and 23 show that the q_{max}/q_y ratio decreases with increase of s. For large values of s, this ratio becomes less than one. Thus, the use of conventional elastic theory may result in unsafe estimates of the load-carrying capacity. This is particularly true for relatively slender arches.

Fig. 24 shows a comparison between the results presented by Harris[16] and authors. Reading off from his figure, Harris's curve is redrawn. The difference between them seem to be very small except nearly symmetrical loading case ($s=0.99$).

4. SUMMARY AND CONCLUSIONS

In this paper a method is presented for the analysis of arches in the elastic and elastic-plastic range. The method takes into account the effects of spread of yielded zones and finite deflections produced by the applied load. The effect of yielding is included in the computations by using the stiffness reduction factors μ and ν. These factors have been developed from the M-N-ϕ-ζ relationships summarized in Tables 1, 2, and 3. The inclusion of finite deflections is accomplished by using the iterative approach shown in Fig. 4. The method has been applied to the analysis of the two-hinged parabolic arch shown in Fig. 7. The load parameter s defines the condition of the applied load.

Numerical analyses were carried out to study the influence of unsymmetrical loading pattern on the strength of arches. Included in the study are arches with rectangular and sandwich cross sections. Additional computations were then performed for arches of different slenderness ratios and rise-to-span ratios. The slenderness ratios selected for the computations are 75, 100 and 150 for the rectangular section arches and 75, 100, 150 and 200 for the sandwich arches. The range of rise-to-span ratio covered is from 0.125 to 0.20.

The following conclusions can be drawn from the results presented in this paper.

1. If the arch remains completely elastic, the load-carrying capacity is almost independent of the loading condition (Fig. 8). The maximum load is governed primarily by elastic buckling.
2. When the effect of yielding is considered, the strength of the arch can be significantly reduced under unsymmetrical loads (Figs. 14 and 18).

3. The deflections in the horizontal and vertical directions have a significant effect on the behavior and strength of slender arches. In general, the load-carrying capacity decreases with increase in slenderness ratio (Figs. 15 and 19).
4. The rise-to-span ratio of the arch also has a significant effect on the maximum load, but the extent of this effect appears to depend on the load parameter s (Figs. 17 and 21).
5. For certain arches, the maximum load can be considerably less than the elastic limit load determined according to the conventional structural theory.

From the numerical results presented, it does not appear possible to express the load-carrying capacity of arches by a simple and general formula, similar to the one available for beam-columns[19]. Further research is necessary in order to develop practical design approaches that will give realistic evaluations of the strength of steel arches.

5. ACKNOWLEDGEMENTS

This study was initiated when the senior author was at Lehigh University as a Foreign Researcher of the Japanese Government. Appreciation is expressed to the members of the Fritz Engineering Laboratory of Lehigh University, especially its Director, Professor Lynn S. Beedle and Dr. S. Morino who provided valuable assistance in computer programming. Thanks are due to Mr. T. Yabuki of the Department of Civil Engineering of Tohoku University for his help in carrying out part of the computations. Miss K. Yoshioka prepared the drawings and typed the drafts of the text. The final manuscript was typed by Miss Karen Philbin.

The computations were performed using the CDC 6400 computer of Lehigh University and NEAC-700 computer of Tohoku University.

6. NOTATIONS

l : span length of arch
L : overall length of arch axis
f : rise of arch
λ : slenderness ratio of arch
A_f : area of flange
I : moment of inertia
A : area
h : depth of cross section
b : width of cross section
q : load intensity factor
q_{max}: maximum load intensity factor which arch can carry
q_p : uniformly distributed load intensity factor at which arch cross section becomes fully plastic at the springings
q_y : load intensity factor at which fiber stress reaches yield stress by the 1st ord. analysis
s : a parameter defining partial loading condition
x : horizontal coordinate divided by l
y : vertical coordinate divided by l
γ : inclination angle of arch axis to horizontal line
v : vertical deflection divided by l
w : horizontal deflection divided by l
Δv : secondary vertical deflection divided by l
Δw : secondary horizontal deflection divided by l
M : bending moment divided by l
ΔM : secondary bending moment divided by l
N : thrust
ΔN : secondary thrust
H : horizontal thrust of arch
ΔH : secondary horizontal thrust of arch
μ : reduction factor for bending stiffness
ν : reduction factor for axial stiffness
E : Young's modulus
E_{st} : strain hardening modulus
σ : stress
σ_y : yield stress
σ_r : residual stress
ε_y : yield strain
ε_{st} : strain at strain-hardening
ε_0 : strain of middle axis of cross section
ε_r : residual strain
ϕ : curvature
ϕ_y : curvature at yielding
M_y : elastic limit moment of rectangular section
N_y : fully plastic thrust of rectangular section
M_p : yield moment of sandwich section
N_p : fully plastic thrust of sandwich section
S_p : $|M|/M_p+|N|/N_p$
D_p : $|M|/M_p-|N|/N_p$

References

1) Dinnik, A. W.: "Buckling and Torsion", Moscow, 1955, p. 160.
2) Stüssi, F.: "Aktuelle baustatische Probleme der Konstruktionspraxis," Schweiz. Bauzeitung, Vol. 106, No. 12, 1935, p. 132.
3) Ratzersdorfer, J.: "Die Knickfestigkeit von

Stäben und Stabwerken", Julius Springer, Vienna, 1936, p. 314.
4) Gaber, E.: "Über die Knicksicherheit vollwandiger Bogen," Bautechnik Nov. 1934, p. 646.
5) Kollbrunner, C. F.: "Versuche über die Knicksicherheit und die Grundschwingungszahl vollwandiger Bogen", Bautechnik, March 1936, p. 186.
6) Deutsch, E.: "Das Knicken von Bogentragern bei unsymmetrischer Belastung", Bauingenieur, Dec. 1940, p. 353.
7) Austin, W. J.: "In-Plane Bending and Buckling of Arches", J. of the Structural Division, ASCE, Vol. 97, No. ST5, 1971, p. 1575.
8) Swida, W.: "Die Berechnung von Stählernen Bögen unter Berücksichtigung der Tragfähigkeitsreserve im elastisch-plastichen Zustand," Der Stahlbau, Vol. 19, No. 3, p. 17, No. 4, p. 29, 1950 and Vol. 20, No. 2, p. 25, 1951.
9) Hendry, A. W.: "The Plastic Design of Two-Pinned Mild Steel Arch Ribs", Civil Engineering and Public Works Review, London, Vol. 47, 1952, p. 38.
10) Johansen, K. W.: "Studies on the Load-Carrying Capacity of Steel Structures", Danish Institute of Technology, Meddelelse, No. 3, 1954.
11) Lange Hansen, P.: "The Carrying Capacity of Curved Beams", Research Laboratory of Building Technique, Technical University of Denmark, Bulletin No. 6, 1956.
12) Steven, L. K.: "Carrying Capacity of Mild Steel Arches", Proc. Institution of Civil Engineers, Vol. 8, 1957, p. 119.
13) Onat, E. T. and Prager, W.: "Limit Analysis of Arches", J. of Mechanics and Physics of Solids, Vol. 1, 1953, p. 73.
14) Onat, E. T. and Shu, L. S.: "Finite Deformations of a Rigid Perfectly Plastic Arch", J. of Applied Mechanics, Vol. 29, 1962, p. 549.
15) Yamazaki, T. and Ishikawa, N.: "Elastoplastic Analysis of Circular Arches", Trans., Japan Society of Civil Engineers, No. 158, 1968.
16) Harries, H.: "Traglasten stählerner Zweigelenkbögen mit ausgebreiteten Fliesszonen", Der Stahlbau, No. 6, p. 170, and No. 8, p. 248, 1970.
17) Maeda, Y. and Fujimoto, K.: "Study on Calculation of Plastic Collapse Load of Two-Hinged Arches", Trans. Japan Society of Civil Engineers, No. 174, 1970.
18) Jezek, K.: "Die Tragfähigkeit axial gedrückter und auf Biegung beanspruchter Stahlstäbe, Der Stahbau, Vol. 9, p. 12, 1936.
19) Column Research Council (U.S.): "Guide to the Design Criteria for Metal Compression Members", 2nd Edition, edited by B. G. Johnston, John Wiley & Sons, p. 160, 1966.

(*Received Dec. 27, 1971*)